

# Central molecular zones in galaxies: $^{13}\text{CO}(6-5)$ and molecular gas conditions in bright nearby galaxies

F.P. Israel<sup>1</sup>, R. Güsten<sup>2</sup>, and A. Lundgren<sup>3</sup>

<sup>1</sup> Sterrewacht Leiden, P.O. Box 9513, 2300 RA Leiden, the Netherlands

<sup>2</sup> Max-Planck-Institut für Radioastronomie, Auf dem Hügel 69, 53121 Bonn, Germany

<sup>3</sup> Aix Marseille Université, CNRS, LAM, Marseille, F-13388, France

Received ???; accepted ???

## ABSTRACT

This paper summarizes all presently available  $J_{\text{upper}} \geq 5$   $^{13}\text{CO}$  and accompanying  $^{12}\text{CO}$  measurements of galaxy centers including new  $J=6-5$   $^{13}\text{CO}$  and  $^{12}\text{CO}$  observations of eleven galaxies with the Atacama Pathfinder EXperiment (APEX) telescope and also *Herschel* high- $J$  measurements of both species in five galaxies. The observed  $J=6-5/J=1-0$   $^{12}\text{CO}$  integrated temperature ratios range from 0.10 to 0.45 in matching beams. Multi-aperture data indicate that the emission of  $^{13}\text{CO}(6-5)$  is more centrally concentrated than that of  $^{12}\text{CO}(6-5)$ . The intensities of  $^{12}\text{CO}(6-5)$  suggest a correlation with those of  $\text{HCO}^+$  but not with those of  $\text{HCN}$ . The new data are essential in refining and constraining the parameters of the observed galaxy center molecular gas in a simple two-phase model to approximate its complex multi-phase structure. In all galaxies except the Seyfert galaxy NGC 1068, high- $J$  emission from the center is dominated by a dense ( $n \sim 10^5 \text{ cm}^{-3}$ ) and relatively cool (20-60 K) high-pressure gas. In contrast, the low- $J$  lines are dominated by low-pressure gas of a moderate density ( $n \sim 10^3 \text{ cm}^{-3}$ ) and more elevated temperature (60-150 K) in most galaxies. The three exceptions with significant high-pressure gas contributions to the low- $J$  emission are all associated with active central star formation.

**Key words.** Galaxies: galaxies: centers – interstellar medium: molecules – millimeter lines – observations

**Table 1.** Line excitation.

$J$ (1)	Frequency (GHz)		$E_u/k^a$ (K)	$n_{\text{crit}}^b$ ( $\text{cm}^{-3}$ )
	(2)	(3)		
	$^{13}\text{CO}$	$^{12}\text{CO}$		
1-0	110.201	115.271	5.5	2e3
2-1	220.399	230.538	16.6	1e4
3-2	330.588	345.796	33.2	4e4
4-3	440.765	461.041	55.3	9e4
5-4	550.926	576.278	83.0	2e5
6-5	661.067	691.473	116.2	3e5
7-6	771.184	806.652	154.9	5e5
8-7	881.273	921.800	199.1	6e5
	$\text{HCN}$	$\text{HCO}^+$		
1-0	88.632	...	4.3	2e5
1-0	...	89.189	4.3	3e4
3-2	265.886	...	25.5	4e6
3-2	...	267.558	25.5	8e5

Notes: a. Jansen (1995); Schöier *et al.* (2005); b. Calculated for kinetic temperatures  $T_{\text{kin}}(\text{CO}) = 100$  K in the optically thin limit ignoring radiative trapping; Carilli & Walter (2013).

## 1. Introduction

Late-type galaxies frequently contain conspicuous central concentrations of molecular gas. These may play an important role in galaxy evolution when they serve as the reservoirs that feed

super-massive black holes, circumnuclear star formation, and massive gas outflows. Various  $^{12}\text{CO}$  ladder surveys, in particular those conducted with the *Herschel* Space Observatory, unambiguously point to the simultaneous presence of both low-pressure and high-pressure gas in these reservoirs (Mashian *et al.* 2015, Kamenetzky *et al.* 2016, 2017, Lu *et al.* 2017, Crocker *et al.* 2019), requiring a multi-phase analysis.

Table 1 illustrates how different molecular line transitions, in principle, can be used to determine molecular gas temperatures and densities. The values in that table were, however, calculated ignoring radiative trapping and assuming optically thin emission, whereas the  $^{12}\text{CO}$ ,  $\text{HCN}$ , and  $\text{HCO}^+$  transitions are optically thick. Significant emission occurs well below the critical density, at densities lower by one or two orders of magnitude (cf. Shirley 2015). Nevertheless, the table provides useful upper limits to the temperature and the density that can be deduced from a transition-limited survey. For instance,  $^{12}\text{CO } J=2-1/J=1-0$  intensity ratios distinguish kinetic temperatures increasingly poorly above 20 K, and  $^{12}\text{CO}$  ladders up to  $J=4-3$  fail to make meaningful distinctions between temperatures above 100 K.

A complication is the degeneracy of optically thick  $^{12}\text{CO}$  ladders with respect to the kinetic temperature, volume density and column density (hence mass) of the gas. A striking illustration of their failure to differentiate between even the very different environmental conditions in NGC 6240 and Mrk 231 is provided by Meijerink *et al.* (2013). Likewise, Weiss *et al.* (2007) found equally good fits to the  $^{12}\text{CO}$  ladders of luminous galaxies but they could not resolve the temperature-density ambiguity. Additional information preferably in the form of optically thin emission from species such as  $^{13}\text{CO}$  is required to alleviate the degeneracy (Bayet *et al.* 2006, Israel 2020, hereafter Paper I). Depending on the available data, two or three gas phases can be

Send offprint requests to: F.P. Israel

modeled. For most purposes, a two-phase analysis suffices as it can be made to fit most of the available observations (e.g., the cases of M 82 and NGC 253 discussed by Loenen et al. 2010 and by Rosenberg *et al.* 2014).

The presently available data on galaxy centers do not constrain the relative amounts of low-pressure and high-pressure gas equally well. In Paper I, we presented a systematical probe of the physical condition of the molecular gas with ground-based surveys of both  $^{12}\text{CO}$  and  $^{13}\text{CO}$  in transitions up to  $J_{\text{upper}} = 4$  and found densities between  $10^2 \text{ cm}^{-3}$  and  $\geq 10^4 \text{ cm}^{-3}$  and temperatures ranging from  $\sim 30 \text{ K}$  to  $\geq 100 \text{ K}$ . The elevated gas temperatures, increased turbulence, and higher metallicities that characterize galaxy centers cause a systematic overestimate of the molecular hydrogen amounts by traditional methods. Instead, the so-called  $X$ -factor relating CO intensities to  $\text{H}_2$  column densities is an order of magnitude lower than the “standard” value in galaxy centers, including the Milky Way center.

These low- $J$  transitions are particularly sensitive to molecular gas of a modest density (cf. Table 1) and constrain the column density and mass of the low-pressure gas relatively well, even though the available line intensities usually do not fully constrain even a two-phase model. In particular, they do not adequately sample the temperatures and densities at the high-pressure end which are much more sensitive to feedback from active-galaxy nuclei (AGN) and from starburst activity. This requires additional surveys of the higher- $J$   $^{12}\text{CO}$  transitions such as those provided by the *Herschel* Spectral and Photometric Imaging Receiver (SPIRE) and Photoconductor Array Camera and Spectrometer (PACS) that cover  $^{12}\text{CO}$  transitions  $J_{\text{upper}} \geq 4$  in a large number of galaxies (e.g., Mashian *et al.* 2015, Rosenberg et al. 2015, Kamenetzky et al. 2016). Such observations were attempted with the *Herschel* Heterodyne Instrument for the Far-Infrared (HIFI) overlapping the few cases where SPIRE sensitivities did also allow the determination of  $^{13}\text{CO}$  line fluxes.

High-frequency observations of extragalactic  $^{13}\text{CO}$  lines are also feasible with ground-based equipment but only at the high-elevation facilities in Hawaii and the Chilean Andes. High atmospheric opacities prevent ground based observation of the  $J=4-3$  and  $J=5-4$   $^{13}\text{CO}$  transitions. The  $^{13}\text{CO}$  line intensities, already low in almost all galaxies, further decrease with increasing  $J$  level. This leaves the  $J=6-5$   $^{13}\text{CO}$  line as the most practical choice to sample the high-excitation gas in galaxy centers from the ground.

## 2. Galaxy sample

The sample considered here includes the few galaxies with *Herschel* detections of  $^{13}\text{CO}$  in  $J_{\text{upper}} \geq 5$  transitions. These concern fluxes extracted from SPIRE spectra covering a great spectral range with low spectral resolution and from targeted Heterodyne Instrument for the Far-Infrared (HIFI) observations with much higher spectral resolution resolving the line profiles. Although SPIRE detected many galaxies in various  $^{12}\text{CO}$  transitions, the weak  $^{13}\text{CO}$  lines were unambiguously detected only in the brightest galaxies on the celestial sky mostly in guaranteed observing time.

The  $^{12}\text{CO}(6-5)$  line was readily observed from the ground, first in the bright galaxies accessible from Hawaii, notably M 82, NGC 253, and IC 342 (Harris *et al.* 1991; Ward *et al.* 2003, Seaquist *et al.* 2006) and in some red-shifted luminous galaxies from lower-elevation sites (cf. Weiss et al. 2007). Less luminous closer galaxies followed (e.g., Bayet *et al.* 2004, 2006), but the ground-based detection of the  $^{13}\text{CO}(6-5)$  line in NGC 253

**Table 2.** Sample galaxies.

Name	R.A. (2000)	Dec. 2000	$V_{\text{LSR}}$	$D$
(1)	h m s	° ' "	$\text{km s}^{-1}$	Mpc
(1)	(2)	(3)	(4)	(5)
Newly observed galaxies				
N253	00:47:33.1	-25:17:18	245	3.4
N613	01:34:18.2	-29:25:06	1480	19.7
N660	01:43:02.4	+13:38:42	843	12.2
N1068*	02:42:40.7	-00:00:48	1135	15.2
N1097*	02:46:19.0	-30:16:30	1270	16.5
N1365*	03:33:36.4	-36:08:25	1635	21.5
N1808	05:07:42.3	-37:30:47	995	12.3
N2559	08:17:06.1	-27:27:21	1560	21.4
N4945*	13:05:27.5	-49:28:06	565	4.4
N5236	13:37:00.9	-29:51:56	515	4.0
N6240	16:52:58.9	+02:24:03	7304	116.4
Galaxies from the literature				
IC342	03:46:48.5	+68:05:47	35	3.5
N3034	09:55:52.7	+69:40:46	275	4.0

Note: Active galaxy nuclei (AGNs) are marked by an asterisk.

(Hailey-Dunsheath *et al.* 2008) so far stood alone. The development of sensitive high-frequency receivers for use in the southern hemisphere provided the opportunity to change this situation. Inspection of the  $J=6-5$   $^{12}\text{CO}$  data in the *Herschel* archive yielded a limited number of galaxies bright enough to attempt  $J=6-5$   $^{13}\text{CO}$  detection from the southern hemisphere without the need for prohibitively long integration times. The sample selected for new observations is listed in Table 2. It includes six galaxies with starburst centers, three have AGN centers, one is the Luminous InfraRed Galaxy merger (LIRG) NGC 6240, and one has a mixed AGN-starburst center (NGC 1365). The two northern galaxies bright enough to have literature mid- $J$   $^{13}\text{CO}$  intensities (M 82 and IC 342) have been included for completeness sake.

## 3. Observations

The observations are part of two separate programs with the Atacama Pathfinder EXperiment telescope (APEX; Güsten *et al.* 2006) at the Llano de Chajnantor high-elevation site in the Chilean Andes. The first series of observations was carried out with the Carbon Heterodyne Array of the MPIfR (CHAMP+) receiver in guaranteed observing time between 2008 and 2012 (projects X-081.F-1002-2008, E-085.B-0094B-2010, E-088.B-0075A.2011, and X-089.F-0007-2012). The second series of observations was carried out with the Swedish-ESO PI instrument for APEX (SEPIA) receiver in 2019 guaranteed observing time and in 2021 regular European southern observatory (ESO) time (projects E-0104.B-0034A-2019 and E-0108.C-0586A.2021). At the observing frequencies of 661.067 GHz ( $^{13}\text{CO}(6-5)$ ), 691.473 GHz ( $^{12}\text{CO}(6-5)$ ) and 806.651/809.350 GHz ( $^{12}\text{CO}(7-6)/[\text{CI}](2-1)$ ) the APEX full-width half maximum (FWHM) beam sizes are 9.3", 8.9" and 7.7" according to the on-line data sheets. Calibration scans on Jupiter and Mars yield efficiencies needed to transform antenna temperatures  $T_A$  into main beam temperatures  $T_{\text{mb}}$  of effectively  $\eta_{\text{mb}} = 0.48, 0.52, \text{ and } 0.48$

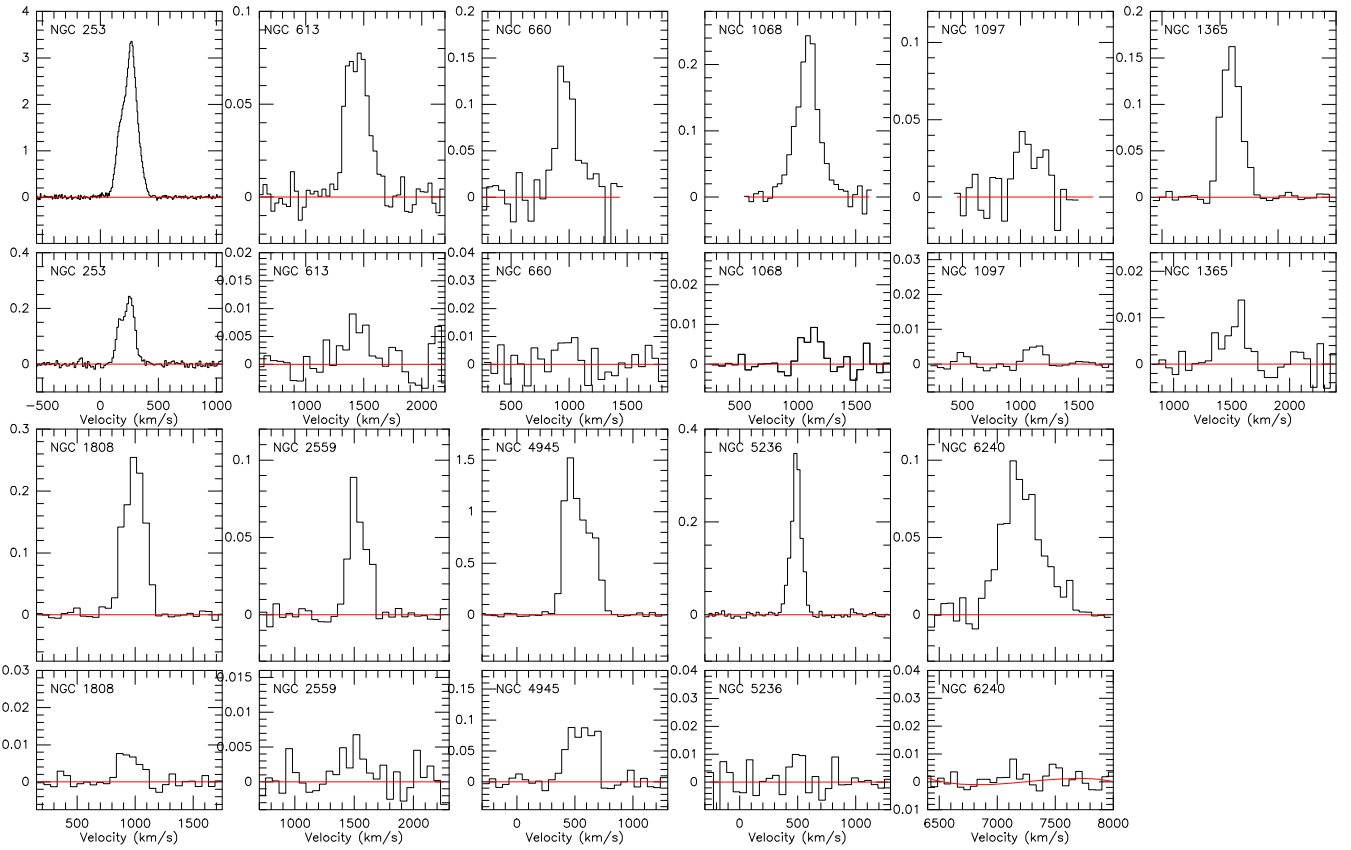


**Fig. 1.** Observed  $J=6-5$   $^{12}\text{CO}$  (top) and  $J=(6-5)$   $^{13}\text{CO}$  (bottom) profiles of galaxy centers. Horizontal scale velocity ( $V_{LSR}$  in  $\text{km s}^{-1}$ , vertical scale observed antenna temperature  $T_{A^*}$ . Note the overall weakness of  $^{13}\text{CO}$  lines.

**Table 3.** Results of APEX observations.

Name	$\int T_{mb} dv$ ( $\text{K km s}^{-1}$ )	$T_{mb}$ (mK)	$\int T_{mb} dv$ ( $\text{K km s}^{-1}$ )	$T_{mb}$ (mK)
(1)	(2)	(3)	(4)	(5)
$^{12}\text{CO}(6-5)^a$				
N253	$1000.4 \pm 2.2$	$5903 \pm 177$	$75.21 \pm 1.08$	$475 \pm 15$
N613	$39.9 \pm 1.6$	$160 \pm 19$	$2.65 \pm 0.71$	$12 \pm 3$
N660	$48.1 \pm 5.2^b$	$252 \pm 37$	$3.79 \pm 1.33$	$21 \pm 5$
N1068	$96.8 \pm 2.9^b$	$444 \pm 51$	$4.46 \pm 0.60$	$21 \pm 3$
N1097	$49.2 \pm 4.1^b$	$90 \pm 22$	$4.48 \pm 1.44$	$13 \pm 4$
N1365	$65.3 \pm 1.2$	$319 \pm 19$	$4.79 \pm 0.65$	$23 \pm 6$
N1808	$64.7 \pm 4.0^b$	$419 \pm 39$	...	...
	$111.5 \pm 1.7$	$498 \pm 38$	$4.63 \pm 0.58$	$17 \pm 5$
N2559	$116.4 \pm 7.1^b$	$404 \pm 41$	...	...
	$29.8 \pm 1.1$	$158 \pm 23$	$2.17 \pm 0.40$	$13 \pm 4$
N4945	$724.0 \pm 6.8$	$2508 \pm 165$	$59.88 \pm 2.88$	$206 \pm 41$
N5236	$68.4 \pm 0.6$	$650 \pm 42$	$3.23 \pm 0.81$	$33 \pm 9$
N6240	$54.7 \pm 2.7$	$148 \pm 18$	$2.21 \pm 0.56$	$6 \pm 2$
$^{12}\text{CO}(7-6)^c$				
[CI](2-1) <sup>c</sup>				
N660	$46.2 \pm 17.5^b$	$691 \pm 252$	$34.3 \pm 18.8$	$333 \pm 219^b$
N1808	$22.2 \pm 2.2^b$	$161 \pm 16$	$36.1 \pm 6.9$	$150 \pm 40^b$
N1068	...	...	$69.0 \pm 8.0$	$335 \pm 57^b$
N1097	...	...	$98.9 \pm 34.4$	$295 \pm 46^b$

Notes: a. SEPIA660 results unless noted otherwise; b. CHAMP+ results; c. binned to the  $9''$  SEPIA660 resolution

with uncertainties of  $0.02^1$ . The conversion factor  $S/T_{mb}$  of flux density  $S$  to brightness temperature  $T_{mb}$  is about  $60 \text{ Jy/K}$ .

### 3.1. CHAMP+ observations

CHAMP+ is a dual-band  $2 \times 7$  element heterodyne array developed by the Max Planck Institute für Radioastronomie (MPIfR) in Bonn (D), the Stichting RuimteOnderzoek Nederland (SRON) in Groningen (NL), and the Jet Propulsion Laboratory (JPL) in Pasadena (USA). It is a principal investigator (PI) instrument operated for the APEX community as a collaborative effort with MPIfR (Kasemann *et al.* 2006, Güsten *et al.* 2008). The array can be operated simultaneously in ALMA (Atacama large millimeter/submillimeter array) bands 9 and 10, and we used this property to obtain carbon  $J=2-1$  [CI] (rest frequency 809 GHz) and  $J=7-6$   $^{12}\text{CO}$  (rest frequency 806 GHz) measurements simultaneously with the Band 9  $J=6-5$   $^{12}\text{CO}$  and  $^{13}\text{CO}$  line measurements. Both sub-arrays have closely spaced pixels in a hexagonal arrangement providing data sampling with half-beam spacing in scanning mode. The backend is an autocorrelator array with a total bandwidth of 32 GHz and 32768 spectral channels, subdivided into 32 IF bands of 1 GHz and 1024 channels each. We used position-switching with a throw of  $900''$ , well clear of the galaxy main bodies. On-the-fly maps were obtained for all sources, mostly with  $50'' \times 50''$  field-of-views. For the purposes of this paper, we extracted single emission profiles by spatially binning all emission within an area corresponding to the desired resolution. The Band 9 data were obtained with sky conditions

<sup>1</sup> [www.mpifr-bonn.mpg.de/4482182/champ\\_efficiencies\\_16-09-14.pdf](http://www.mpifr-bonn.mpg.de/4482182/champ_efficiencies_16-09-14.pdf), [www.apex-telescope.org/telescope/efficiency/](http://www.apex-telescope.org/telescope/efficiency/)

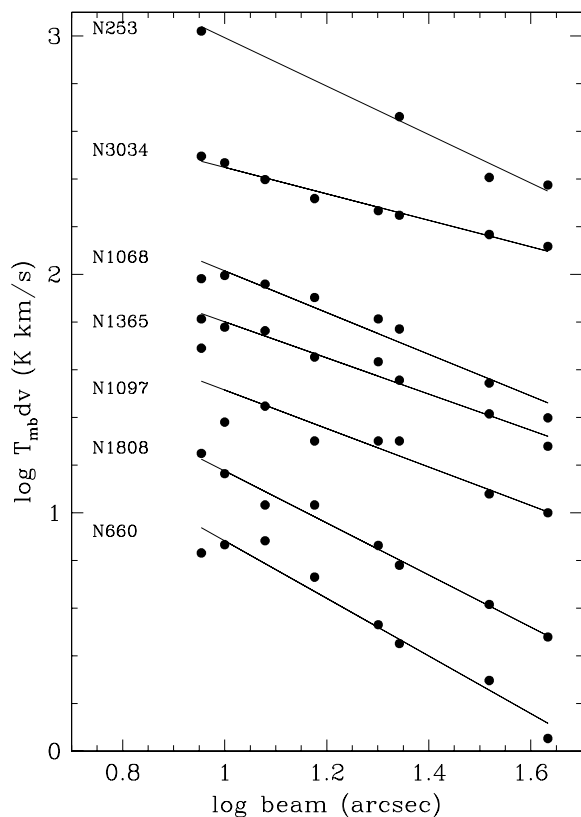


**Fig. 2.** Integrated  $^{12}\text{CO}(6-5)$  line intensities as a function of aperture. For clarity sake, points for NGC 1808 and NGC 660 were shifted down by 0.80 and 0.85, respectively. Solid lines are least-squares fits to the data. Six galaxies have poor data coverage and are not shown. NGC 613, IC 342, and NGC 2559 have a single data point each. NGC 4945, NGC 5236, and NGC 6240 have only two data points each.

varying from good (total system temperature including sky  $T_{\text{sys}} = 840$  K) to just acceptable ( $T_{\text{sys}} = 1675$  K). In Band 10, total system temperatures varied from 2400 to 4000 K. The calibration is estimated to be accurate to  $\leq 30\%$ . This error is almost entirely governed by baseline uncertainties. The emission from the observed galaxies typically occupies about half of the  $1200 \text{ km s}^{-1}$  window covered by the backend and leaves limited room for accurate baseline definition. The baseline errors are too large to derive reliable fluxes for the weak  $^{13}\text{CO}$  emission.

### 3.2. SEPIA observations

The (SEPIA) is a single-pixel heterodyne receiver with a cryostat accommodating three ALMA-like receiver cartridges (Belitsky *et al.* 2018), provided by the group for advanced receiver development (GARD) at the Onsala space observatory (S). We used the SEPIA660 cartridge (Baryshev *et al.* 2015), which is a dual polarization 2SB receiver installed and commissioned by the Groningen NOVA group (NL) during the second half of 2018. The SEPIA660 receiver covers the window between 597 GHz and 725 GHz. It has two IF outputs per polarization, USB and LSB, each covering 4-12 GHz, adding up a total of 32 GHz instantaneous IF bandwidth. The central frequencies of the two side-bands are separated by 16 GHz. The backend was an

**Table 4.** Beam-dependent  $^{12}\text{CO}(6-5)$  intensities.

(1)	Intensity $I(\text{CO}) = \int T_{\text{mb}} dv$ ( $\text{K km s}^{-1}$ )				Fit Parameter <sup>a</sup>		Ratio <sup>b</sup>
	9''	22''	33''	43''	$a$	$b$	(6-5)/(1-0)
N253 <sup>c</sup>	1049	459	255	237	-1.00	3.97	0.45±0.05
N660	48	20	14	8	-1.08	2.94	0.13±0.02
N1068	96	59	35	25	-0.85	2.83	0.35±0.05
N1097	49	20	12	10	-0.81	2.32	0.15±0.03
N1365	65	36	26	19	-0.76	2.56	0.14±0.02
N1808	112	38	26	19	-1.13	3.12	0.28±0.05
N3034 <sup>d</sup>	313	177	147	131	-0.56	3.02	0.26±0.03
N4945 <sup>e</sup>	724	...	130	...	-0.74	...	0.20±0.04
N5236	68	...	...	10	-1.22	...	0.12±0.03
N6240	55	...	...	10	-1.09	..	0.30±0.1

Notes: a. slope  $a$  and intercept  $b$  a resulting from fitting of observed intensities as a function of beamsize:  $\log(\text{intensity}) = a \log(\text{beam}) + b$ . b.  $J=1-0$  data from Paper I; c. 40'' from *Herschel*-HIFI (Pérez-Beaupuits *et al.* 2018); d. Convolved *JCMT* data (Seaquist *et al.* 2006); 33'' *Herschel*-HIFI from (Loenen *et al.* 2010); e. 33'' from *Herschel*-HIFI data (Bellochi *et al.* 2020).

FFT spectrometer with a spectral resolution of about 61 kHz (26 m/s) with 65536 channels per every 4 GHz. For NGC 253 and NGC 4945 we obtained a five-point cross on the central position in  $^{12}\text{CO}$ ; all other observations were single pointings. The sky conditions mostly varied from very good ( $T_{\text{sys}} = 500 - 700$  K) to good ( $T_{\text{sys}} = 700 - 1100$  K). Throughout the observations, the baselines were quite stable and the (much) wider velocity coverage allowed good baseline definition and subtraction.

### 3.3. Additional observations

In the following discussion, we also include the mid- $J$   $^{13}\text{CO}$  observations of bright galaxies that already exist in the literature. These concern spaceborne and ground-based detections of NGC 253 (Hailey-Dunsheath *et al.* 2008, Pérez-Beaupuits *et al.* 2018), IC 342 (Rigopoulou *et al.* 2013), NGC 3034 (M 82; Loenen *et al.* 2010, Panuzzo *et al.* 2010, Kamenetzky *et al.* 2012), NGC 5128 (Centaurus A; Israel *et al.* 2014) and NGC 4945 (Bellochi *et al.* 2020).

## 4. Results and analysis

### 4.1. Extracted $^{12}\text{CO}$ line intensities

The velocity-integrated and peak  $J=6-5$   $^{12}\text{CO}$  and  $^{13}\text{CO}$  line intensities measured with the CHAMP+ and SEPIA660 receivers are listed in Table 3. The table also lists the  $J=7-6$   $^{12}\text{CO}$  and  $J=2-1$  [CI] fluxes measured with the CHAMP+ receiver in parallel with the  $J=6-5$  observations. To facilitate comparison, we have binned these higher frequency data to the somewhat lower spatial resolution of the  $J=6-5$  measurements. The errors listed are stochastic errors; they do not include systematic errors due to calibration etc. For NGC 1365 and NGC 1808  $^{12}\text{CO}$  intensities were available from both the CHAMP+ and the SEPIA660 receiver on APEX. Comparison shows a good agreement between the results obtained with the different receivers on different occasions. In spite of the different observing techniques, there is

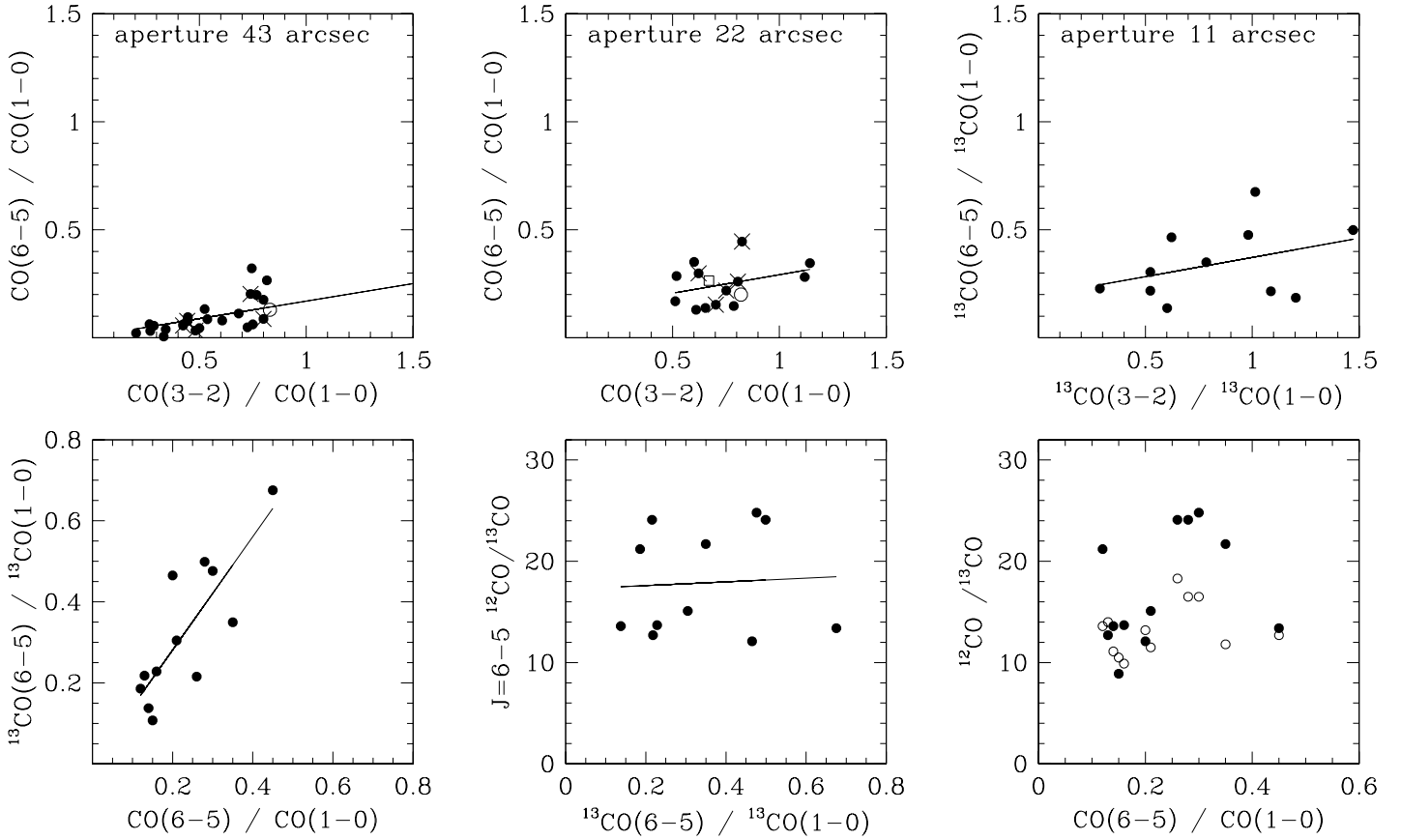


**Fig. 3.** Comparison of observed line ratios. Straight lines mark least-squares linear fits to the data displayed. Top row: comparison of  $J=6-5$  and  $J=3-2$  line intensities normalized by  $J=1-0$  intensity. Left:  $^{12}\text{CO}$  ratios in  $43''$  apertures. Open circle marks the Inner Galaxy including Galactic Nucleus. Center:  $^{12}\text{CO}$  ratios in  $22''$  apertures. Open circle marks the Galactic Center; open square marks the starburst dwarf galaxy He2-10. In both panels, the relatively nearby galaxies at distances  $D \leq 6.5$  Mpc are marked by a cross. Right:  $^{13}\text{CO}$  ratios in extrapolated  $11''$  apertures. Bottom row: comparison of isotopologue intensities in (extrapolated)  $11''$  apertures. Left: comparison of the  $^{13}\text{CO}$  and  $^{12}\text{CO}$   $J=6-5/J=1-0$  intensity ratios. Center: comparison of the  $J=6-5$  isotopologue intensity ratios and the  $^{13}\text{CO}$   $J=6-5/J=1-0$  intensity ratios. The outlier NGC 6240 is not included. Right: isotopologue intensity ratios as a function of  $^{12}\text{CO}(6-5)/^{12}\text{CO}(1-0)$  intensity ratios. The  $J=1-0$  isotopological ratios are assumed to be identical in  $11''$  and  $22''$  apertures. Filled circles mark isotopological intensity ratios in the  $J=6-5$  transition, open circles those in the  $J=1-0$  transition.

likewise good agreement, for the three galaxies observed with *Herschel*/SPIRE that were also mapped with APEX/CHAMP+. In comparable apertures, the CHAMP+ fluxes are 20 per cent higher for both NGC 1068 and NGC 1097 and 20 per cent lower for NGC 1365. The galaxies NGC 660 and NGC 1808 were not observed with SPIRE.

Five of the sample galaxies are relatively close to our Galaxy with distances  $D=3.4-4.5$  Mpc (Table 2). At microwave frequencies, they are among the brightest galaxies in the sky. Three of them (NGC 253, M 82, and NGC 4945) accordingly have  $^{12}\text{CO}(6-5)$  intensities an order of magnitude higher than the other galaxies in the survey, including those at the same distance (IC 342 and M 83). The remaining eight galaxies have  $^{12}\text{CO}$  intensities similar to the latter although they are at three to five times greater distance, thirty times greater in the case of the ultra-luminous galaxy NGC 6240. A similar pattern applies to

the considerably weaker  $^{13}\text{CO}(6-5)$  fluxes that required integration times up to several hours.

In ten of the thirteen galaxies of the sample,  $^{12}\text{CO}(6-5)$  intensities were measured at different spatial resolutions. They either have multiple pointed observations in the different SEPIA660, HIFI and SPIRE apertures, or they were mapped, for instance with the CHAMP+ receiver, which allowed extraction of intensities binned to various resolutions  $\theta$ . The results for individual galaxies are shown in Fig. 2 together with fits to the data of the form  $\log(T_{mb}dv) = a \log(\theta) + b$ . In this formulation,  $a=0$  corresponds to an extended source of constant surface brightness and  $a = -2$  corresponds to a point source. Intensities at the various resolutions in the narrow range  $-0.75 \geq a \geq -1.2$  ( $9''$  to  $43''$ ) are listed in Table 4 together with the fit coefficients  $a$  (slope) and  $b$  (intercept). The nearly edge-on galaxy NGC 3034 (M 82) has a flat slope  $a = -0.56$  caused by a relative lack of  $^{12}\text{CO}(6-5)$  emission from the center (see Seaquist *et al.* 2006, Loenen

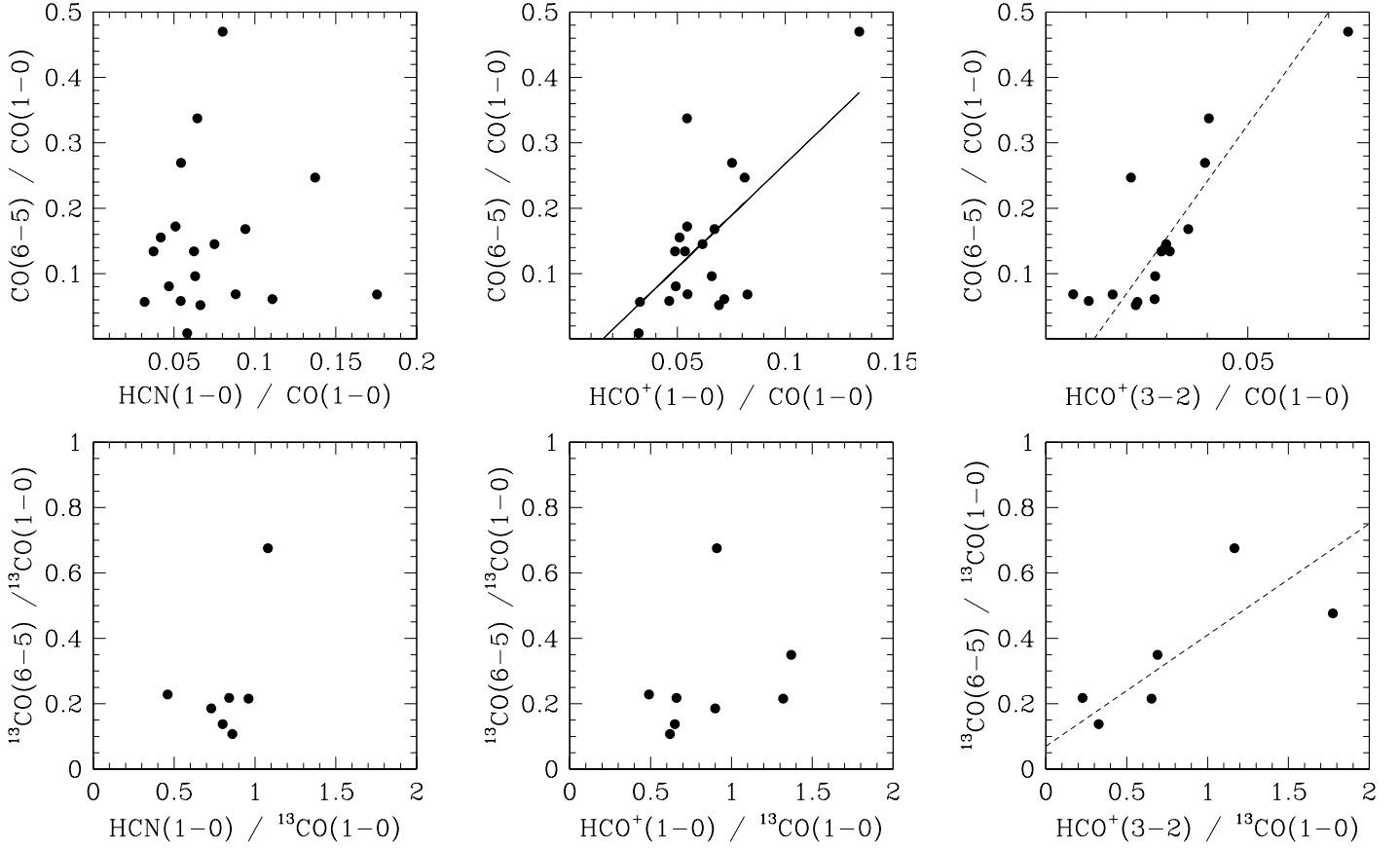


**Fig. 4.** Top:  $^{12}\text{CO}(6-5)/(1-0)$  intensity ratios as a function of HCN(1-0),  $\text{HCO}^+$  and  $\text{HCO}^+(3-2)$  line intensities relative to  $^{12}\text{CO}(1-0)$ . All ratios refer to a resolution of  $22''$ , except the  $^{13}\text{CO}(6-5)/(1-0)$  ratios that refer to extrapolated  $11''$  apertures (cf. section 4.3). The central and rightmost panels include linear fits to the data. Bottom: the same as the top row, but with  $^{13}\text{CO}$  lines substituted for  $^{12}\text{CO}$  lines. The dashed line in the rightmost panel is an eyeball fit to the limited data

**Table 5.** APEX  $^{12}\text{CO}/^{13}\text{CO}$  isotopologue intensity ratios.

Name	$J=6-5^a$ ( $9''$ )	$J=3-2^b$ ( $14''$ )	$J=2-1^c$ ( $11''$ )	$J=1-0^c$ ( $22''$ )
(1)	(2)	(3)	(4)	(5)
N253	$13.3 \pm 0.2^d$	$11.7 \pm 1.2$	$10.7 \pm 1.1$	$12.7 \pm 1.3$
N613	$15.1 \pm 4.4$	$11.3 \pm 2.1$	$10.5 \pm 2.1$	$11.5 \pm 1.8$
N660	$12.7 \pm 3.3$	$12.4 \pm 1.9$	$19.8 \pm 2.4$	$14.0 \pm 1.4$
N1068	$21.7 \pm 3.2$	$15.2 \pm 2.2$	$12.8 \pm 1.4$	$11.8 \pm 1.7$
N1097	$11.0 \pm 3.7$	$14.6 \pm 2.3^e$	$14.4 \pm 2.2$	$10.5 \pm 1.6$
N1365	$13.6 \pm 2.0$	$12.2 \pm 1.3$	$11.7 \pm 1.2$	$11.1 \pm 1.5$
N1808	$24.1 \pm 3.3$	$17.1 \pm 1.7$	$12.9 \pm 1.4$	$16.5 \pm 1.2$
N2559	$13.7 \pm 2.7$	$22.4 \pm 4.3$	$10.4 \pm 2.1$	$9.9 \pm 1.9$
N4945	$12.1 \pm 0.6$	$7.5 \pm 0.9^f$	$7.7 \pm 0.9^g$	$13.2 \pm 1.3$
N5236	$21.2 \pm 5.3$	$10.0 \pm 1.2$	$8.3 \pm 1.3$	$13.6 \pm 1.1$
N6240	$24.8 \pm 6.8$	$26.5 \pm 6.6$	$38 \pm 9.4$	$29 \pm 8$

Notes: a. APEX, This Paper; b. JCMT, Paper I; c. IRAM, Paper I; d. CSO ( $11''$ ), Hailey-Dunsheath *et al.* (2008); e. APEX,  $18''$  Piñol-Ferrer *et al.* (2011); f. APEX ( $18''$ ) Bellocchi *et al.* (2020); g. SMA ( $10''$ ) Chou *et al.* (2007);

**Table 6.** Herschel  $^{12}\text{CO}/^{13}\text{CO}$  isotopologue intensity ratios.

Name	$J=5-4$ ( $35''$ )	$J=6-5$ ( $33''$ )	$J=7-6$ ( $36''$ )	$J=8-7$ ( $40''$ )
(1)	(2)	(3)	(4)	(5)
N253 <sup>a</sup>	$18 \pm 1$	$25 \pm 8$	$29 \pm 11$	$30 \pm 12$
IC342 <sup>b</sup>	$11 \pm 3$	$26 \pm 8$	...	...
N3034 <sup>c</sup>	$19 \pm 4$	$24 \pm 2$	$30 \pm 6$	$34 \pm 10$
N4945 <sup>d</sup>	$14 \pm 3$	$22 \pm 2$	$18 \pm 2$	...
Cen A <sup>e</sup>	$19 \pm 2$	...	...	...

Notes: a. SPIRE, Pérez-Beaupuits *et al.* (2018); b. SPIRE, Rigopoulou *et al.* (2013); c. HIFI, Loenen *et al.*, (2010); SPIRE, Panuzzo *et al.* (2010), Kamenetzky *et al.* (2012); d. HIFI, Bellocchi *et al.* (2020); SPIRE, Bellocchi private communication (2021); e. HIFI, Israel *et al.* (2014).

*et al.* 2010) but the remainder has an average slope  $a = -0.92$ . A similar inverse proportionality between intensity and aperture in the central regions of galaxies was also found, with larger dispersion, for low- $J$  emission from the  $^{12}\text{CO}$  molecule (Paper I)

as well the HCN and  $\text{HCO}^+$  molecules that trace molecular gas with critical densities similar to those of the  $^{12}\text{CO}(6-5)$  transition (Israel 2023, hereafter Paper II). Such behavior is characteristic for the centrally peaked emission from galaxies illustrated in Figure 3 of Paper I. No dependence on distance is apparent. The average  $a=-0.9$  of the nearby galaxies NGC 253, NGC 3034, NGC 4945, and NGC 5236 only samples the central 0.7-0.9 kpc. The intensities of the more distant galaxies (except NGC 6240) sample the significantly larger inner regions with diameters of 2.6-4.5 kpc, yet have the same average  $a=-0.9$ .

#### 4.2. $J=6-5$ $^{12}\text{CO}/^{13}\text{CO}$ intensity ratios

The APEX survey provides direct determination of the  $J=6-5$   $^{12}\text{CO}/^{13}\text{CO}$  intensity ratio at a resolution of  $9''$  in the eleven galaxies listed in Table 5. The table includes the corresponding  $J=3-2$ ,  $J=2-1$ , and  $J=1-0$  ratios in apertures covering surface areas larger by factors of 2.4, 15, and 6.0, respectively (Paper I). The  $J=1-0$  to  $J=3-2$  intensity ratios are typically 10-15 in all galaxies except NGC 6240. In seven galaxies the  $J=6-5$  and  $J=1-0$  ratios do not significantly differ. In the other galaxies, the  $J=6-5$  ratio exceeds the  $J=1-0$  ratio by a factor of up to two. Four galaxies have relatively high  $J=6-5$  ratios. The intensity ratios of the LIRG NGC 6240 are the highest in the sample. Papadopoulos *et al.* (2014) suggest even higher ratios for this galaxy. These and other literature ratios have, however, large uncertainties because the very weak and broad  $^{13}\text{CO}$  lines are highly sensitive to baseline errors. Measurements with *Herschel* provide additional  $J=5-4$  to  $J=8-7$  intensity ratios for five more galaxies at the substantially lower resolutions of  $33''$ - $43''$  listed in Table 6, thereby sampling surface areas twelve to twenty times larger than covered by the APEX beam. The large-aperture  $^{12}\text{CO}/^{13}\text{CO}$  intensity ratios in the  $J_{\text{upp}} \geq 6$  transitions in Table 6 are two to three times higher. The  $J=5-4$  intensity ratio is transitional, with an in-between average of  $\sim 16$ . The large-area *Herschel*  $J=6-5$  ratios vary little, ranging between 22 and 26, and are similar to the four highest  $J=6-5$  ratios in the APEX sample. For NGC 253 and NGC 4945,  $J=6-5$  ratios are available in both apertures. In the fifteen times larger surface area sampled by *Herschel*, the  $J=6-5$  isotopologue ratio has increased from the APEX value  $\sim 13$  to the almost twice higher value of 23. In these two galaxies, the  $^{13}\text{CO}$  intensities are thus much weaker beyond the inner 200 pc and even more centrally peaked than the  $^{12}\text{CO}$  intensities. At least half (six out of thirteen) of the galaxies surveyed exhibits  $J_{\text{upp}} \geq 6$  intensity ratios of 20-30 in either small or large apertures. By analogy, this could also be the case for the other galaxies in Table 5 lacking *Herschel*  $^{13}\text{CO}$  data.

We can take this a step further for NGC 253 and NGC 4945. After subtraction of the contribution by the inner circumnuclear area (APEX) to the larger central area (*Herschel*), the intensity ratio in the residual  $9''$ - $33''$  zone of either galaxy becomes  $^{12}\text{CO}(6-5)/^{13}\text{CO}(6-5) \sim 40$ , suggesting low optical depths also for  $^{12}\text{CO}$ . Together with ratios in excess of 20-30 in transitions with  $J_{\text{upp}} \geq 6$  this is consistent with intrinsic  $[^{12}\text{CO}]/[^{13}\text{CO}]$  isotopologue abundances of about 40 (cf. Tang *et al.* 2019, Viti *et al.* 2020), as assumed in our earlier Papers I and II on circumnuclear molecular gas.

#### 4.3. Further line ratio comparisons

In these papers, we adopted a “standard” aperture of  $22''$  for intercomparison of the observed line intensities. For the galaxy centers in this paper, we obtained such normalized  $^{12}\text{CO}(6-5)$

intensities in a  $22''$  aperture either by direct determination or interpolation from Table 4, or by extrapolating the observed  $9''$  intensities from Table 3 with the average slope  $a=-0.9$  just determined (NGC 613, IC 342, and NGC 2559). These are directly comparable to the  $22''$   $J_{\text{upp}} \leq 4$  line intensities (Paper I) of the same galaxies. In Fig. 3 (top) we show relations between  $^{12}\text{CO}$  line ratios constructed from these data. We also plotted transition intensity ratios in the  $43''$  apertures of a larger sample of twenty galaxies using the  $^{12}\text{CO}$  intensities compiled by Kamenetzky *et al.* (2016) and Paper I. Nine galaxies are common to both samples. For comparison we added the nearby starburst dwarf galaxy He2-10 (data from Bayet *et al.* 2006) as well as both the inner Milky Way and the Galactic Center (data from Fixsen *et al.* 1999)

As noted in section 4.2, comparison of the data in Tables 5 and 6 suggests a strong aperture-dependency of the  $^{12}\text{CO}/^{13}\text{CO}$  ratio. In order to limit the extrapolation as much as possible, we have adopted for this case a common aperture of  $11''$ . We assume identical distributions for the  $J=6-5$  emission in the  $^{13}\text{CO}$  and  $^{12}\text{CO}$  lines over this small range. If instead the  $^{13}\text{CO}(6-5)$  emission is point-like, its normalized intensity is overestimated by  $\sim 15\%$ . For the normalization of the  $^{13}\text{CO}(1-0)$  intensity we assumed emission aperture ratios identical to those in the  $J=2-1$  transition (Paper I). In a similar way we extrapolated the  $^{13}\text{CO}(3-2)$  data from  $14''$  to  $11''$ .

The  $^{13}\text{CO}(6-5)$  intensities are not so easily normalized to a  $22''$  aperture because only a single point per galaxy is observed at a resolution of  $9.5''$ . In order to minimize aperture-dependent effects we have limited the extrapolation to an aperture of  $11''$  and we assumed identical distributions for the emission in the *thirco* and  $^{12}\text{CO}$  lines over this small range. If instead the  $^{13}\text{CO}(6-5)$  emission is point-like, its normalized intensity is overestimated by  $\sim 15\%$ . For the normalization of the *thirco*(1-0) intensity we assumed instead emission aperture ratios identical to those in the  $J=2-1$  transition (Israel 2020). In a similar way we extrapolated the  $^{13}\text{CO}(3-2)$  data over the small range of  $14''$  to  $11''$ . In Figure 3 (bottom) we show the relations of the isotopologues to each other and to the  $J=6-5$  and  $J=1-0$  transitions.

#### 4.4. Excitation of the $^{12}\text{CO}(6-5)$ gas

Studies of the  $^{12}\text{CO}$  rotational ladders of galaxy centers have been published by several authors (Bayet *et al.* 2006, Weiss *et al.* 2007, eve *et al.* 2014, Rosenberg *et al.* 2015, Mashian *et al.* 2015, and Kamenetzky *et al.* 2016) to which we refer for further detail. In these studies, the rotational ladders are primarily interpreted in terms of excitation and the heating and cooling balance of the gas. The SPIRE and PACS  $^{12}\text{CO}$  ladders (Rosenberg *et al.* 2015, Mashian *et al.* 2015) illustrate the great variety in overall shape. This variety is already apparent in the line intensity ratios shown in the top left and center panels of Fig.3. The excitation represented by the (6-5)/(1-0) and the (3-2)/(1-0)  $^{12}\text{CO}$  ratios varies for the galaxies in our sample in a manner not related to galaxy type. The excitation of the emission in these transitions increases significantly with decreasing aperture size. The trend is continued when  $^{13}\text{CO}$  line intensity ratios observed at even higher resolution are plotted (Fig. 3 top right). The two ratios are weakly correlated (slope  $a=0.17 \pm 0.09$ ). The systematic displacements imply that the excitation of the central molecular gas increases towards the galaxy nucleus.

The panels in the bottom row of Fig. 3 show the relations of the isotopological  $^{12}\text{CO}$  and  $^{13}\text{CO}$  intensities to each other and to the  $J=6-5/J=1-0$  transitions ratios. Although the LIRG

NGC 6240 was observed, we exclude it from most of the following analysis as its extreme distance, surface area measured, and luminosity class (see e.g., Greve *et al.* 2009, Papadopoulos *et al.* 2014) set it too far apart from the other galaxies in the sample. For the other galaxies, there is a clear relation between the  $^{13}\text{CO}$  and  $^{12}\text{CO}$  ladders (bottom left panel) but the intensity ratio of the (6-5) and (1-0) transitions increases more rapidly for the optically thin  $^{13}\text{CO}$  than for the optically thick  $^{12}\text{CO}$ . On the other hand, the  $J=6-5$   $^{12}\text{CO}/^{13}\text{CO}$  isotopological intensity ratio is not correlated with the intensity ratio of the  $J=6-5$  and  $J=1-0$   $^{13}\text{CO}$  or  $^{12}\text{CO}$  transition that track the gas excitation nor is the  $J=1-0$   $^{12}\text{CO}/^{13}\text{CO}$  isotopological intensity ratio (bottom center and bottom right panels).

The critical density of  $^{12}\text{CO}(6-5)$  is similar to that of  $\text{HCN}(1-0)$  and falls in between those of  $\text{HCO}^+(1-0)$  and  $\text{HCO}^+(3-2)$ , (see Table 1, so that a mutual comparison may be of interest. Again, we normalize all line intensities by the  $^{12}\text{CO}(1-0)$  intensity. Fig. 4 explores the behavior of  $J=6-5$   $^{12}\text{CO}$  and  $^{13}\text{CO}$  lines as a function of the  $\text{HCN}(1-0)$ ,  $\text{HCO}^+(1-0)$  and  $\text{HCO}^+(3-2)$  intensities (data from this paper and from Papers I and II). In all panels, the most extreme (6-5)/(3-2)  $^{12}\text{CO}$  ratios belong to NGC 6240 (high) and NGC 5055 (low). No correlation is apparent between the  $\text{HCN}(1-0)$  and either  $^{12}\text{CO}(6-5)$  or  $^{13}\text{CO}(6-5)$  line intensities (Fig. 4, leftmost panels) or  $\text{HNC}(1-0)$  (not shown) despite their very similar critical densities. There is, perhaps, a correlation between the  $^{12}\text{CO}(6-5)$  and  $\text{HCO}^+(1-0)$  line emission (top center panel) and, more convincingly in spite of the few data points available, between  $\text{HCO}^+(3-2)$  and  $^{12}\text{CO}(6-5)$  and even  $^{13}\text{CO}(6-5)$  (rightmost top and bottom panels). This suggests that  $\text{HCO}^+$  is linked to the excitation of high- $J$   $^{12}\text{CO}$  and  $^{13}\text{CO}$  (but see also Papadopoulos *et al.* 2010) and  $\text{HCN}$  is not. This is consistent with the poor sensitivity of the  $\text{HCN}/\text{CO}$  intensity ratios to both column density and fraction of dense gas noted by Priestley *et al.* (2024) in molecular cloud simulations and by Israel (2023) in extragalactic multi-transition molecular line surveys. Although the heating and cooling of extragalactic molecular gas can be determined from the observed  $^{12}\text{CO}$  ladders, this is not so easily the case for its physical parameters temperature, density, column density as these are highly degenerate. Single-gas-phase models in general do not adequately explain even relatively uncomplicated extragalactic  $^{12}\text{CO}$  ladders and models with two or more distinct gas components are needed (e.g., Greve *et al.* 2014, Mashian *et al.* 2015, Kamenetzky *et al.* 2016). This need had already been recognized in the analysis of multiple low- $J$  transitions of optically thick  $^{12}\text{CO}$  complemented by optically thin  $^{13}\text{CO}$  transitions (for instance Israel 2001, 2005; Bayet *et al.* 2006).

## 5. Molecular gas physics revealed by $J=6-5$ CO lines

The objects in this paper were all included in the previously published survey of the  $J=1-0$ ,  $J=2-1$ ,  $J=3-2$  transitions of  $^{12}\text{CO}$  and  $^{13}\text{CO}$  emission from galaxy centers whereas for half the sample the  $J=4-3$   $^{12}\text{CO}$  transition was also measured (Paper I). The results of that survey were evaluated with large-velocity-gradient (LVG) models employing the *RADEX* radiative transfer code (Van der Tak *et al.* (2007). For the details of the analysis we refer to section 5 of Paper I. The LVG approximation efficiently solves the radiative transfer equation in non-LTE environments and yields a first order determination of the gas properties in a homogeneous medium. For each case, the model provides an average description of all the molecular gas in the aperture, thus lumping together gas of all temperatures and densities. As the

number of gas phases included is increased, the models become ever more realistic. The *RADEX* analysis, however, requires four input parameters per phase and per species ( $\text{H}_2$  kinetic temperature and density, molecular column density per velocity interval, relative molecular abundance). Even with simplifying assumptions (such as identical  $\text{H}_2$  temperature and density for all species), the number of phases that can be ltaneously modeled is severely limited by the number of independent measurements. In the case of the low- $J$   $^{12}\text{CO}$  and  $^{13}\text{CO}$  measurements presented in our previous work only two gas-phases can be modeled. This allows a first, coarse separation of the dominant gas components, such as dense or diffuse, and cool or warm. Although a simplification of reality, this is nevertheless already a great improvement on single-phase models that produce averages with little physical meaning. A complication is that for each gas phase, the observed line intensities are always subject to degeneracies between temperature, density, and column density per velocity interval. These degeneracies are not always clearly resolved by the limited number of transitions providing independent line intensities especially when finite errors are taken into account. Instead of a well-constrained unique result, the two-phase modeling produced for each galaxy a number of possible solutions. These form a well-defined and limited range of physical parameters; examples are given in appendix C.1 of Paper I. With only low- $J$  transitions, the number of independent measurements is usually sufficient only to marginally constrain the seven parameters needed to describe two phases, producing tight constraints for some parameters but leaving others practically unconstrained. Fits with a cut-off at the  $J=3-2$  or  $J=4-3$  transitions tend to underestimate the parameters of the high-pressure gas, in particular the density. Biased fit results for the high-pressure gas in turn influence the fit parameters of the low-pressure gas, especially the temperature.

This is borne out by the new measurements in the  $J=6-5$  transition. For each galaxy the various physical parameter sets that provide good fits to the  $J_{\text{upp}} \leq 3$  intensity ratios, including the “best” fits listed in Table C.2 of Paper I, fail to adequately predict the line intensities observed in the  $J=6-5$  transition. The observed  $^{12}\text{CO}$  intensities generally exceed the model-predicted values by factors of two or more.

For  $^{13}\text{CO}(6-5)$ , the result is no better. Even in galaxies where the predicted 22” model isotopologue intensity ratios are broadly similar to the observed 9” APEX ratios this is only because the individual  $^{12}\text{CO}$  and  $^{13}\text{CO}$  intensities are both off by the same factor. Thus, the observations of the lower  $J=1-0$ ,  $J=2-1$ , and  $J=3-2$  transitions alone do not sufficiently constrain the modeling of gas physical parameters to also allow successful prediction of the higher  $J=6-5$  transition intensities. The new  $J=6-5$   $^{12}\text{CO}$  and especially  $^{13}\text{CO}$  observations provide information on the physical condition of the molecular gas not apparent in the lower- $J$  measurements.

This has major consequences for the modeling presented in Paper I. The addition of two more intensities increases the number of independent parameters to the number required to fully describe the two gas phases. The number of possible parameter sets derived from the  $J_{\text{upp}} \leq 3$  analysis for each galaxy is drastically reduced. To agree with the  $J_{\text{upp}} = 6$  data, at least one of the two model phases needs to have a kinetic temperature of 60 K or higher, and at least one of the two phases needs to have a density of  $10^4 \text{ cm}^{-3}$  or higher. Sets falling short of this criterion can be removed – this includes all but a few of the sets that were earlier found to provide possible solutions in the analysis described in Paper I. The  $J_{\text{upp}} \leq 3$  measurements very poorly distinguish temperatures and densities much above these values (cf. the effective upper limits in Table 1). High model temperatures and



**Table 7.** Physical parameters from molecular gas modeling.

Name (1)	Density $n(\text{H}_2)$ ( $\text{cm}^{-3}$ ) (2)	Gas parameters		Pressure parameter $nT$ ( $\text{cm}^{-3}$ K) (5)	Fractional emission		mass (8)	Model combined intensity ratios		
		Temperature $T_{\text{kin}}$ (K) (3)	Gradient $N_{\text{CO}}/dv$ ( $\text{cm}^{-2}/\text{km s}^{-1}$ ) (4)		$^{12}\text{CO}(1-0)$ (6)	$^{12}\text{CO}(6-5)$ (7)		$^{12}\text{CO}$ (6-5)/(1-0) (9)	$^{12}\text{CO}/^{13}\text{CO}$ $J=1-0$ (10)	$J=6-5$ (11)
NGC 253	1e5	30	1.5e17	3e6	0.08	0.97	0.30	0.48	13	13
	3e3	150	3e16	4.5e5	0.92	0.03	0.70			
NGC 613	1e5	60	1e17	6e6	0.15	0.97	0.23	0.21	11	12
	1e3	30	6e16	3e4	0.85	0.03	0.77			
NGC 660	5e4	60	1e17	3e6	0.12	0.84	0.19	0.15	13	16
	1e3	60	6e16	6e4	0.88	0.16	0.81			
NGC 1068	1e5	20	3e17	2e6	0.03	0.02	0.02	0.37	12	27
	3e3	150	3e17	4.5e5	0.97	0.98	0.98			
NGC 1097	1e5	60	6e16	6e6	0.09	0.87	0.06	0.16	10	13
	5e2	60	1e17	3e4	0.91	0.13	0.94			
NGC 1365	5e4	60	1e17	3e6	0.12	0.84	0.19	0.15	13	16
	1e3	60	6e16	6e4	0.88	0.16	0.81			
IC 342	1e5	20	1e17	2e6	0.88	0.91	0.96	0.21	10	17
	3e3	150	3e16	4.5e5	0.12	0.10	0.04			
NGC 1808	1e5	60	3e16	6e6	0.09	0.67	0.03	0.28	13	33
	1e3	150	1e17	1.5e5	0.91	0.33	0.97			
NGC 2559	1e5	60	6e16	6e6	0.09	0.87	0.06	0.16	10	13
	5e2	60	1e17	3e4	0.91	0.13	0.94			
NGC 3034	1e5	100	1e17	1e7	0.07	0.74	0.07	0.27	12	16
	1e3	100	1e17	1e5	0.93	0.26	0.93			
NGC 4945	1e5	25	1e17	2.5e6	0.52	0.92	0.67	0.20	16	20
	1e3	100	3e16	1e5	0.48	0.08	0.33			
NGC 5236	1e5	20	1e17	2e6	0.46	0.84	0.58	0.12	13	27
	1e3	100	3e16	1e5	0.54	0.16	0.42			

(column) densities from the initial analysis need fine-tuning to fit the  $J=6-5$  values without compromising the low- $J$  line ratios.

Still assuming a  $[^{12}\text{CO}]/[^{13}\text{CO}]$  isotopic abundance ratio of 40 (Tang *et al.* 2019, Viti *et al.* 2020), we revised the two-phase models of the sample galaxies from Paper I to accommodate the new  $J=6-5$  intensities. The newly determined parameters of the two phases are summarized in columns 2, 3 and 4 of Table 7. For each galaxy, two entries are given that refer to the respective high-pressure (top) and the low-pressure phase (bottom) identified in column 5. Columns 6 through 8 list the fractions of the total  $^{12}\text{CO}(1-0)$  and  $^{12}\text{CO}(6-5)$  emission and the mass associated with each gas phase. Finally, columns 9 through 11 show the  $J=6-5$   $^{12}\text{CO}$  and  $^{13}\text{CO}$  model line ratios for the combined emission from the two phases. These can be compared to the observed (6-5)/(1-0) ratios listed in Table 3 and the isotopologue intensity ratios in Tables 5 and 6. We did not remodel NGC 6240 as it is incomparable to the other galaxies in terms of distance, area covered, and luminosity class (see e.g., Greve *et al.* 2009, Papadopoulos *et al.* 2014).

The inclusion of the  $J=6-5$  measurements thus results in fits that are much more tightly constrained than those based on the  $J_{\text{upp}} \leq 4$  transitions only. This is largely due to the  $^{13}\text{CO}$  intensities that render the isotopological intensity ratios particularly sensitive to changes in the physical parameters. Most of the solutions allowed by the analysis in Paper I are completely ruled out by the present analysis. There remains a small residual uncertainty due to the limited ability to distinguish between temperatures above 200 K and densities well in excess of  $10^5 \text{ cm}^{-3}$ .

For two-phase models, much of the ambiguity previously present is eliminated. Other parameter combinations are still possible but only as long as they are close to those listed in

Table 7. It is, however, unfeasible to assign uncertainties to individual parameters because of the trade-offs inherent in degeneracies. Instead, we assign very roughly a factor of two uncertainty to the overall result. An additional source of uncertainty is the actual  $^{12}\text{CO}/^{13}\text{CO}$  abundance. Values as low as 30 and as high as 70 have been published but most determinations settle around 40 which is the value we assumed. If in any galaxy the abundance is different, this would lead to modestly different model parameters. We note that such a situation seems to apply to luminous infrared galaxies such as NGC 6240 with abundances of 100-200.

The two-phase model fits presented here provides a simplified but robust picture of the molecular gas in the sample galaxies, especially as concerns the division in gas of high and low pressure. They are, however, still a first approximation and not yet a fully realistic description of that gas. Nevertheless, the agreement with similar results derived independently by others is encouraging. From the analysis of CS emission ladders in half a dozen galaxies Bayet *et al.* (2009), for instance, conclude to the general presence of two high-pressure phases with kinetic temperatures all below 70 K, with similar densities  $0.4-1.6 \times 10^5 \text{ cm}^{-3}$  for the dominant cold high-pressure phase but with higher densities  $2.5-40 \text{ times } 10^5 \text{ cm}^{-3}$  for the more sparse warm high-pressure phase. The galaxy NGC 253 also provides an interesting case for comparison, because it has been comprehensively analyzed by Rosenberg *et al.* (2014) and Pérez-Beaupuits *et al.* (2018), using all available  $^{12}\text{CO}$ ,  $^{13}\text{CO}$ , HCN, [CI], and [CII] lines to fit three distinct gas components. The results listed for the phases of NGC 253 in Table 7 are within a factor of two of the results for the corresponding phases in these two analyses.

Compared to our earlier analysis by Paper I, the new results in Table 7 show either similar or moderately higher temperatures and densities for the low-pressure gas forced by the new high-pressure values. The high-pressure gas temperatures are also roughly similar but the densities are revised up, in most cases significantly, in order to reproduce the observed intensities of the  $^{12}\text{CO}(6-5)$  and especially the  $^{13}\text{CO}(6-5)$  lines. Uncertainties are much reduced.

The low-pressure gas is not very dense ( $500\text{--}3000\text{ cm}^{-3}$ ) but tends to be hot with kinetic temperatures from 60 K to 150 K. The high-pressure gas is always very dense ( $0.5\text{--}1.0 \times 10^5\text{ cm}^{-3}$  or higher) and significantly cooler with temperatures ranging from 20 K to 60 K. Only in NGC 3034 (M 82) both gas phases have similar temperatures of about 100 K.

Two of the twelve galaxies in Table 7 stand out with gas of a single phase responsible for essentially all of their CO line emission. Hot, moderately dense low-pressure gas produces over 95% of the emission from the center of NGC 1068 independent of transition observed, but a small amount of cold, dense gas is still required to explain the data. Having observed the lower transitions of HCN,  $\text{HCO}^+$  and CO isotopologues with the arcsecond-sized *SMA* and *NOEMA* beams, Krips *et al.* (2011) obtained a very similar result. Almost all of the emission arises from the gas within  $\sim 150$  pc from the active Seyfert nucleus only resolved by interferometer arrays. The circumnuclear gas in the starburst-dominated center of IC 342 is also of limited extent but here it is the high-pressure gas that provides almost all of the CO line emission from this nearby nucleus. The cool and very dense gas in this reservoir produces typically 90% of the CO emission again independent of observed transition. Only ten per cent of the gas in the IC 342 nuclear region is moderately dense but rather hot which was also concluded by Rigopoulou *et al.* (2013), see also Montero-Castaño *et al.* (2006).

In two other galaxies, NGC 4945 and NGC 5236 (M 83), both warm and modestly dense low-pressure gas and much more dense and colder high-pressure gas contribute in roughly equal amounts to the  $J=1-0$  CO groundstate emission. Similar to IC 342, these are relatively nearby galaxies and the line measurements sample only the gas reservoirs in the inner few hundred parsecs. In the likewise nearby galaxies NGC 253 and NGC 3034 (M 82) the high-pressure gas is, however, only a minor contributor to the groundstate CO emission as is also the case in the other six galaxies.

Thus, the  $J=1-0$   $^{12}\text{CO}$  emission from all but three of the observed galaxy centers primarily originates in low-pressure gas reservoirs. More than 85 per cent of the groundstate emission from these galaxies which dominates their molecular gas mass represents moderately dense gas at kinetic temperatures above 60 K and reaching as high as 150 K. Both temperature and density suggest a heating mechanism other than UV and are more compatible with mechanical heating from decaying shocks and turbulent dissipation. Infrared spectroscopy with *Herschel* and *Spitzer* already suggested this for NGC 1097 (Beirão *et al.* 2012).

In all galaxies except NGC 1068 the situation is completely reversed in the  $J=6-5$  transition. More than 85 per cent of the  $^{12}\text{CO}(6-5)$  emission in these galaxy centers comes from relatively cool but rather dense molecular gas reservoirs in most cases representing a minor fraction of the total mass.

The high-pressure gas has an optical depth of a few in the  $J=6-5$  transition. Although it is radiatively important, its source of excitation is not clear-cut as various mechanisms may compete as discussed, for instance, by Rosenberg *et al.* (2014) for the case of NGC 253. If the high- $J$   $^{12}\text{CO}$  emission originates in

thin outer layers of molecular clouds, it could trace high-density gas excited by external UV radiation. The low temperature, the angular extent of the  $^{12}\text{CO}(6-5)$  emission and the apparent lack of accompanying  $^{13}\text{CO}$  emission in NGC 253 and NGC 4945 are, however, more consistent with an extended diffuse gas excited throughout its entire volume by mechanical heating (see Loenen *et al.* 2008, Kazandjian *et al.* 2015, Paper II).

## 6. Conclusion

In this paper we have summarized all fourteen presently available sets of  $J_{\text{upp}} \geq 5$   $^{13}\text{CO}$  measurements of galaxies beyond the Local Group. Together with the more abundant  $^{12}\text{CO}(6-5)$  measurements, they yield thirteen  $J=6-5$   $^{12}\text{CO}/^{13}\text{CO}$  isotopologue ratios for comparison with  $J_{\text{upp}} \leq 3$  ratios established earlier. The distances of the sample galaxies range from 3.5 to 21.5 Mpc. We also observed the LIRG NGC 6240 at a distance of 116 Mpc but did not include it in the analysis because of its discrepant nature. We have determined  $^{12}\text{CO}(6-5)$  intensities in multiple apertures ranging from  $9''$  to  $43''$  in ten galaxies. On average, the surface brightness of the galaxies in this sample is roughly inversely proportional to aperture size, indicating centrally peaked emission. The  $^{12}\text{CO}(6-5)$  emission reduced to  $22''$  apertures is relatively bright with velocity-integrated  $(6-5)/(1-0)$  brightness temperature ratios ranging from 0.12 to 0.45. A wider sample of galaxies observed in a  $43''$  aperture yields on average significantly lower ratios of  $(6-5)/(1-0)$ , suggesting that the larger apertures include a higher fraction of low-excitation gas and that molecular gas excitation increases towards galaxy nuclei. Line intensities of  $^{12}\text{CO}(6-5)$  and  $^{13}\text{CO}(6-5)$  are weakly correlated with those of  $\text{HCO}^+$  and not at all with those of HCN, although all three lines have similar (critical) densities and presumably kinetic temperatures.

This paper not only covers all extragalactic  $^{13}\text{CO}(6-5)$  measurements available to date but, by implication, also all available intensity ratios  $J=6-5$   $^{12}\text{CO}/^{13}\text{CO}$  that can be compared to those of the lower  $J_{\text{upp}} \leq 3$  transitions. These ratios are the emission-weighted average of a variety of molecular cloud types ranging from dense and compact to tenuous and diffuse over relatively large areas. In about a third of the galaxies observed, the isotopologue intensity ratios vary little with transition, in the remaining two thirds the  $J=6-5$  ratio is notably higher than the ratio in the lower transitions seen in somewhat larger apertures. In four galaxies, ratios determined in the fifteen times larger *Herschel* aperture increase with observed transition to much higher values of typically 30. The increase to high values occurs around the  $J=5-4$  transition.

The actual  $^{12}\text{CO}$  and  $^{13}\text{CO}$  intensities in the  $J_{\text{upp}} \geq 6$  transitions are not easily predicted from the  $J_{\text{upp}} \leq 3$  transitions routinely available from ground based facilities. The low- $J$  and high- $J$  lines originate in different and mostly unrelated gas phases. Widely accessible  $^{12}\text{CO}$  line intensities in the  $J=1-0$  through  $J=3-2$  transitions fail to fully constrain these gas phases even when they are accompanied by complementary  $^{13}\text{CO}$  observations. We find from our two-phase RADEX models that additional  $^{13}\text{CO}$  line intensities in the  $J=6-5$  transition or higher eliminate much of the degeneracy and consequent uncertainty in the underlying physical parameters of the molecular gas. For the majority of galaxies the models indicate that most of the observed  $J=6-5$   $^{12}\text{CO}$  and  $^{13}\text{CO}$  emission arises in a warm ( $T_{\text{kin}} \geq 20\text{K}$ ) and very dense ( $n_{\text{H}_2} \gtrsim 10^5\text{ cm}^{-3}$ ) gas. The observed  $J=6-5$  CO emission is important as a tracer of inner galaxy energetics but not as a tracer of inner galaxy molecular gas mass.

*Acknowledgements.* We gratefully acknowledge the ESO APEX User support supplied by Carlos de Breuck. We thank Enrica Bellocchi for supplying us with the *Herschel*-SPIRE intensities of NGC 4945 in Table 6, and Dimitra Rigopoulou for communicating the *Herschel*-SPIRE data for IC 342 in advance of publication.

## References

- Baryshev, A. M., Hesper, R., Mena, F. P., and 24 co-authors, 2015, *A&A* 577, A129
- Bayet, E., Gerin, M., Phillips, T.G., & Contursi, A., 2004, *A&A* 427, 45
- Bayet, E., Gerin, M., Phillips, T.G., & Contursi, A., 2006, *A&A* 467, 485
- Bayet, E., Aladro, R., Martín, S., Vitim S., & Martín-Pintado, J., 2009, *ApJ* 707, 126
- Beirão, P., Armus, L., Helou, G., and 39 co-authors, 2012, *ApJ* 751, 144
- Belitsky, V., Lapkin, I., Fredrixon, M., and 31 co-authors, 2018, *A&A* 612, A23
- Bellocchi, E., Martín-Pintado, J., Güsten, T., and 8 co-authors, 2020, *A&A* 642, A166
- Carilli, C. L. & Walter, F. 2013, *ARAA* 51, 105
- Chou, R.C.Y., Peck, A.B., Lim, J., and 6 co-authors, 2007, *ApJ* 670, 116
- Crocker, A.F., Pellegrini, E., Smith, J.-D. T., and 16-co-authors, 2019, *ApJ* 887, 105
- Fixsm, D.J., Bennett, C.L., & Mather, J.C., 1999, *ApJ* 526, 207
- Greve, T.R., Papadopoulos, P.P., Gao, Y., & Radford, S.J.E., 2009, *ApJ* 692, 1432
- Güsten, R., Nyman, L.A., Schilke, P., and 3 co-authors, 2006, *A&A* 454, L13
- Güsten, R., Baryshev, A., Bell, A., and 26 co-authors, 2008, in Society of Photo-Optical Instrumentation Engineers (SPIE) Conference Series, Vol. 7020, Society of Photo-Optical Instrumentation Engineers (SPIE) Conference Series
- Harris, A.I., Hills, R.E., Stutzki, J., and 3 co-authors, 1991, *ApJL* 382, L75
- Hailey-Dunsheath, S., Nikola, T., Stacey, G.J., and 5 co-authors, 2008, *ApJL* 689, L109
- Israel, F.P., & Baas, F., 2001, *A&A* 371, 433
- Israel, F.P., 2005, *A&A* 438, 855
- Israel, F.P., Güsten, R., Meijerink, R., and 8 coauthors, 2014, *A&A* 562, A96
- Israel, F.P., 2020, *A&A* 635, A131 (Paper I)
- Israel, F.P., 2023, *A&A* 671, A59 (Paper II)
- Jansen, D., 1995, Ph.D. thesis, Sterrewacht, Leiden University (NL)
- Kamenetzky, J., Glenn, J., Rangwala, N., and 14 co-authors, 2012, *ApJ* 753, 70
- Kamenetzky, J., Rangwala, N., Glenn, J., Maloney, P.R., & Conley, A., 2016, *ApJ* 829, 93
- Kamenetzky, J., Rangwala, N., & Glenn, J., 2017, *MNRAS* 471, 2917
- Kasemann, C., Güsten, R., Heyminck, S., and 7 co-authors, 2006, Presented at the Society of Photo-Optical Instrumentation Engineers, *Proc. SPIE* 6275
- Kazandjian, M., Meijerink, R., Pelupessy, F.I., Israel, F.P., & Spaans M., 2015, *A&A* 574, A127
- Krips., M., Martín, S., Eckart, A., and 11 co-authors, 2011, *ApJ* 736, 37
- Loenen, A.F., Spaans, M., Baan, W.A., & Meijerink, R., 2008, *A&A* 488, L5
- Loenen, A.F., van der Werf, P.P., Güsten, R., and 23 co-authors, 2010, *A&A* 521, L21
- Lu, N., Zhao, Y., Díaz-Santos, and 18 co-authors, 2017, *ApJS* 230, 1
- Mashian, N., Sturm, E., Sternberg, A., and 16 co-authors, 2015, *ApJ*, 802, 81
- Meijerink, R., Spaans, M., & Israel, F.P., 2007, *A&A* 461, 793
- Meijerink, R., Kristensen, L.E., Weisz, A., and 28 co-authors, 2013, *ApJL* 762, L16
- Montero-Castaño, M., Herrnstein, R.M., & Ho, P.T.P., 2006, *ApJ* 646, 919
- Panuzzo, P. Rangwala, N., Rykala, A., and 60 co-authors, 2010, *A&A* 518, L37
- Papadopoulos, P.P., van der Werf, P., Isaak, K., & Xilouris, E.M., 2010, *ApJ* 715, 775
- Papadopoulos, P.P., Zhang, Zhi-Yu, Xilouris, E.M., and 6 co-authors, 2014, *ApJ* 788, 153
- Pérez-Beaupuits, Güsten, R., Harris, A., and 5 co-authors, 2018, *ApJ* 860, 23
- Piñol-Ferrer, N., Fathi, K., Lundgren, A., van de Ven, G., 2011, *MNRAS* 414, 529
- Priestley, F.D., Clark, P.C., Golver, S.O.C., and 4 co-authors, 2024, *MNRAS* in press, arXiv:2406.06702
- Rigopoulou, D., Hurley, P.D., Swinyard, B.M., and 9 co-authors, 2013, *MNRAS* 434, 2051
- Rosenberg, M.J.F., Kazandjian, M.V., van der Werf, P.P., Israel, F.P., Meijerink, R., and 3 co-authors, 2014, *A&A* 564, A126
- Rosenberg, M.J.F., van der Werf, P.P., Aalto, S., Armus, L., Charmandaris, V., and 25 co-authors, 2015, *ApJ* 801, 72
- Schöier, F.L., van der Tak, F.F.S., van Dishoeck E.F., & Black, J.H. 2005, *A&A* 432, 369, Leiden Atomic and Molecular Database
- Shirley, Y.L., 2025, *PASP* 127, 299
- Seaquist, E.R., Lee, S.W., & Moriarty-Schieven, G.H., 2006, *ApJ* 638, 148
- Tang, X.D., Henkel, C., Menten, K.M., and 16 co-authors, 2019, *A&A* 629, A6
- van der Tak, F.F.S., Black, J.H., Schöier, F.L., and 2 co-authors, 2007 *A&A* 468, 627
- Viti, S., Fontani, F., & Jiménez-Srra, I., 2020, *MNRAS* 497, 4333
- Ward, J.S., Zmuidzinas, J., Harris, A.I., Isaak, K.G., 2003, *ApJ* 587, 171
- Weiss, A., Downes, D., Walter, F., & Henkel, C., 2007, *AS PC*, 375, 25